Research Article

Antiopi-Malvina Stamatellou*

PZT and PVDF piezoelectric transducers' design implications on their efficiency and energy harvesting potential

https://doi.org/10.1515/ehs-2022-0087
Received July 31, 2022; accepted September 7, 2022;
published online September 21, 2022

Abstract: Despite the intensive research carried out in the last two decades, the actual performance of piezoelectric energy harvesters needs significant improvement for widespread applicability. Custom designed experimental set-ups and methods can be applied for the evaluation of new piezoelectric energy harvesters or modified design versions of existing transducers, in terms of efficiency and specific power. In this context, two representative types of commercial cantilever piezoelectric transducers, made of PZT and PVDF material respectively, were tested in various combinations of aerodynamic and harmonic base excitation. A line type laser was used along with long exposure photography for the visualisation of the piezofilm's mode shapes, tip deflection and the digitization of the elastic line at the oscillation extrema. The harvested power was measured at on-resonance conditions and studied relative to the excitation combinations and the mode shapes. Energy conversion efficiency, defined as the ratio of the electric-field energy accumulated by the supercapacitors, over the total elastic strain energy change of the material during the oscillations is measured and compared. Design improvements are proposed for both transducer types to extract and absorb higher amounts of energy and improve their bandwidth to match the available excitation source characteristics.

Keywords: harvesting efficiency; piezoelectric transducers; PVDF; PZT; transducer design.

***Corresponding author: Antiopi-Malvina Stamatellou**, Mechanical Engineering Department, University of Thessaly, Volos 38334, Greece, E-mail: malvina@uth.gr. https://orcid.org/0000-0002-8108-0115

Introduction

Energy harvesting can be useful in powering low power electronics, reducing the need for battery replacement, maintenance and recharging, by exploiting ambient energy in industrial environments, where there is also a need for sensor networks that ensure the components' optimal operation. Powering by energy harvesters enables the installation of more sensors and the placement of sensors in places where wiring is not feasible. The design of wireless sensor network (WSN) nodes powered by piezoelectric energy harvesters (PEHs) is under study with temperature sensing being a relevant application (Wang et al. 2020). Energy harvesters can complementarily power wireless devices and decrease battery replacement frequency. Piezoelectric energy harvesting (PEH) is the most popular energy harvesting concept exploiting ambient kinetic energy through vibration from engines, heavy equipment, highways and railways (Priya et al. 2017). Possible applications include autonomous condition monitoring of rotating machinery (Khazaee et al. 2019), health monitoring of aerospace structures (Elahi 2021) and self-powered medical implants (Mayekol Mayck et al. 2021). The main disadvantage of PEHs is the limited power output when the excitation frequency is far from the transducer's resonance frequency and efforts are made to broaden their operation bandwidth, or provide for a self-tuning capability (Aboulfotoh and Twiefel 2017; Aboulfotoh et al. 2017; Brenes et al. 2020; Fan, Ghayesh, and Lu 2020). PEHs can also be excited with flow-induced vibration. PEHs tend to vibrate on their eigen-frequency when subjected to air flow (Stamatellou and Kalfas 2020). Flutter type PEHs are elastic films clamped at their leading edge and free at their trailing edge. The flow excitation has been realized by Karman vortex street created by bluff bodies (Tam Nguyen, Pham, and Wang 2013). Harvesters employing new concepts with flow-induced vibration have been presented such as the use of sliding bluff bodies to increase the power output (Sun and Seok 2020), nested bluff-body structures in tandem arrangements (Sun, Guo, and Seok 2019) and coupling of vortex-induced vibration and galloping phenomena. A variation of the flutter type

of harvester is the inverted piezoelectric flag (Kim et al. 2013) employed in autonomous wind speed measurement (Orrego et al. 2017). Flapping is a desired state for the piezoelectric film in piezoelectric energy harvesting, as it increases the acting stresses and thus the output energy. Piezoelectric energy harvesters can be profitably excited through a combination of base and flow induced vibration (Bibo and Daqaq 2013; Dai, Abdelkefi, and Wang 2014). An important parameter in this context is their energy conversion efficiency, which is critical for the design optimization of PEHs and is employed to compare PEHs with alternative power generation systems. It is defined as the ratio of the output energy to the input energy of a system. For a PEH this is the ratio between the output electrical energy and the input mechanical energy. As discussed in (Yang, Erturk, and Zu 2017), this definition has some similarity to the k_{ij}^2, where k_{ij} is the material coupling factor, reported by the manufacturers of piezoelectric material, to show how efficiently the piezoelectric material converts strain energy into electrical energy, not taking into account the specific structural design and rectification circuit. The overall harvester efficiency is usually much smaller than the material coupling factor k_{ij}. Various expressions for the input and output energy have been proposed, and this could be a reason for the large discrepancy in efficiency values reported. Shu and Lie (Shu and Lien 2006) theoretically analyzed the energy conversion efficiency, at the system's level, of a cantilever PEH coupled with a full-bridge rectifier around resonance states. They assumed that the input mechanical energy was the sum of extracted electrical energy and the energy dissipated by the structure damping. According to their definition, efficiency depends on the frequency ratio $\tilde{\omega}$ (response frequency/natural frequency), the normalized resistance α, a system's electromechanical coupling coefficient, k_e^2, (defined in terms of the three system's variables: effective piezoelectric coefficient Θ, a spring's effective stiffness k_{sp} and capacitance C_P) and the mechanical damping ratio ζ. Thus, efficiency increases with a high coupling coefficient and a small damping ratio. Since the coupling coefficient is inversely proportional to the bending stiffness and the internal piezoelectric capacitance, designs with thin films and small internal capacitance are more efficient harvesters. Most experimental studies of PEHs efficiency lack an energy saving circuit and their findings on the expected power output are vast estimations. In this study, an existing testing and assessment methodology is applied to two different types of piezoelectric film transducers, excited, where possible, with both aerodynamic and base excitation. Output voltage is rectified and charges a super capacitor array. The LDT1-028K was selected as representative PVDF transducer, based on its proven performance (Stamatellou and Kalfas 2018, 2020). A versatile test rig was employed to provide the necessary aerodynamic and base excitation (Stamatellou and Kalfas 2019). Power density and conversion efficiency are measured in selected, optimal excitation modes, in terms of base vibration frequency, flow velocity field and the transducer's deflection at oscillations extrema (Stamatellou and Kalfas 2021). The same setup is employed to comparatively study a PZT transducer, namely, the S128-J1FR-1808-YB in a range of base vibration frequencies near the resonant frequency. The detailed design of the two transducers is taken into account in the strain energy calculations.

Methods

Transducers' samples

The S128-J1FR-1808-YB is a 71.1 × 25.4 × 0.71 mm PZT 5J, 1-Layer Bender with Sealed Mounting (Figure 1a). It is a single layer piezoelectric actuator (unimorph) placed between two 30 μm copper electrodes, which collect the charge and transmit it to the terminals. Bending of the composite beam produces curvature where the piezo layer is alternately under tension or compression, according to the curvature sign. It is essential that the piezo layer is not in the neutral axis of the composite beam, to avoid signal cancellation. Two Fire Retardant 4 (FR4) epoxy laminate reinforcement layers (shims) enclose the sensitive piezoelectric ceramic. The thickness of the PZT is 0.15 mm out of the total 0.66 mm transducer's thickness (Figure 1a). The basic design of the LDT1-028K commercial piezoelectric film transducer is also presented in Figure 1b, for comparison. It is made of a single layer of the fluoropolymer Polyvinylidene Fluoride (PVDF) laminated between a Mylar film layer and a thin acrylic coating (Vatansever et al. 2011).

Both transducers are subjected to bending and the stress is mainly in direction 1. Polarization of the PVDF film is done in direction 3. Stresses 1–3 are normal and 4–6 are shear. The general macroscopic geometrical and mechanical properties of the composite transducer's construction are compared in Table 1. The physical properties pertaining to the PZT-5J and the PVDF material, respectively, which determine the piezoelectric behaviour of the respective transducers, are comparatively presented in Table 2.

A comparison of mechanical and thermal properties of PVDF, Mylar and Acrylic with the respective properties of the PZT-5J, FR4 and the copper electrode material, is presented in Table 3.

Testing setup

The piezoelectric energy harvesting test rig comprises the two excitation sources, the piezoelectric transducer and the rectification and energy storage circuit (Figure 2). The two exciters were: a) a 120 W centrifugal fan that created a controlled aerodynamic excitation and b) a cone speaker that created a sinusoidal base excitation. This is a commercial cone speaker (50 W rms, 4 Ω impedance and 180 mm diameter) that converted into oscillating motion the sinusoidal input signal produced

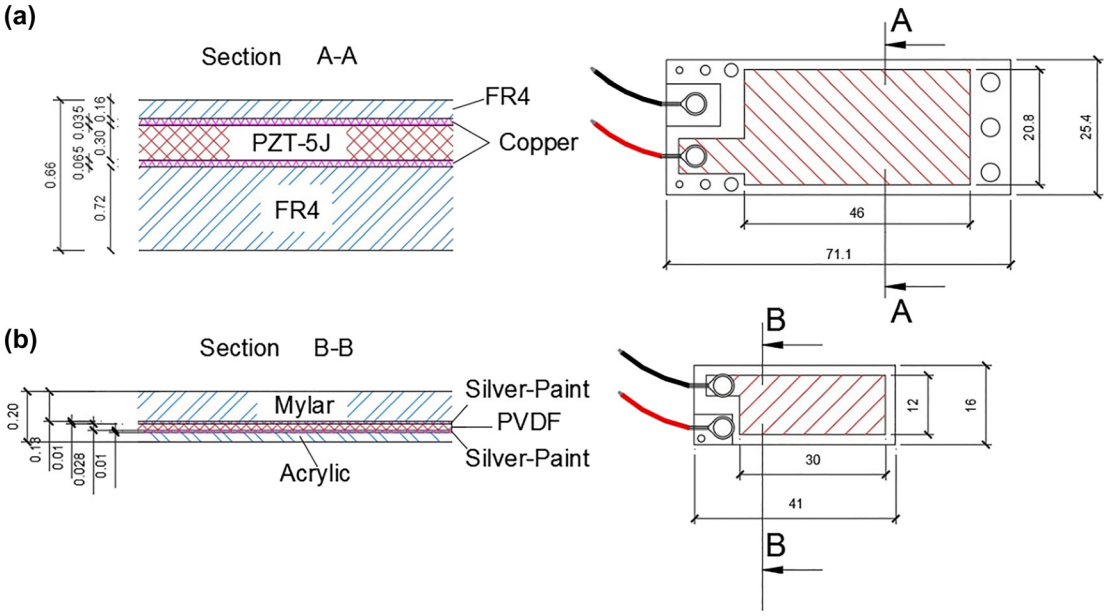

Figure 1: Comparative design – main dimensions and section of laminated structure of (a) the PZT transducer S128-J1FR-1808-YB (Carter and Kensley 2020) and (b) the PVDF transducer LDT1-028K (Measurement_Specialties 2008).

Table 1: General specifications of the PZT transducer S128-J1FR-1808-YB and the PVDF transducer LDT1-028K with reference to the composite structure (Measurement_Specialties 2008).

Parameter	PVDF (LDT1)	PZT (S128)
Length (mm)	41	71.1
Width (mm)	16	25.4
Thickness (mm)	0.20	0.66
Mass (g)	0.5	3.0
Capacitance (nF)	1.38	100
Spring constant based on tip force (N/mm)	0.005	0.306
Resonant frequency (Hz)	58	134

Table 2: Piezoelectric properties of the PZT-5J material (Carter and Kensley 2020) and the PVDF material (Nix and Ward 1986).

Property	Symbol	PZT-5J	PVDF	Units
Dielectric permittivity (1 kHz)	K_3^T	2.35×10^{-8}	107×10^{-12}	F/m
Dielectric loss factor (1 kHz)	tanδ	0.02	0.01	–
Coupling coefficients	k_t	0.53	0.1	–
	k_{33}	0.74	0.20	–
	k_{31}	0.45	0.09	–
Piezoelectric charge (displacement coefficient)	d_{31}	−270	21	pCb/N
	d_{33}	485	−32.5	pCb/N
	d_{15}	850	−27	pCb/N

by the signal generator and amplified through a vacuum tube pre-amplifier and a 2 × 25W (rms) main amplifier.

The same test rig, shown in Figure 3, is employed for both transducers. Both piezoelectric transducers are mounted in a cantilevered horizontal position, on a wooden base fixed on the dust cap at the center of the cone speaker. The transducer's tip is at 40 mm distance from the fan's exit throughout the flow excitation experiments. Fan speed was varied by an inverter from 1320 to 2640 rpm. For the specific set-up, the dimensionless bending stiffness is in the range between 0.1 and 0.25 for the PVDF sensor. The respective range for the PZT transducer is two orders of magnitude higher, which is not favorable for flow induced excitation. A modification of the PVDF transducer to change its resonance frequency, was made by the installation of a magnetic tip mass of 0.78 g, consisting of two small pieces of NdFeB magnet. A KBP 206 rectifying bridge is connected to the transducer's output. The bridge's output was connected to a 1.66 F super capacitor (6 × 2.7 V, 10 F capacitors, connected in parallel). The use of super capacitors in the rectification and energy storage circuit is proven to be beneficial to the efficiency of these devices (Krishnamoorthy et al. 2020; Lu et al. 2020; Ramadoss et al. 2015). The use of super capacitors keeps a low voltage output throughout the testing duration that is comparable to the voltage levels required for charging lithium batteries and power various types of sensors and wireless emitters. Voltage measurements were performed with a 16-bit 400 kSa/s Data Acquisition Board (USB 6212, National Instruments). The DAQ board is connected at the output of a KBP 206 rectifying bridge, in parallel with the super capacitor array that stores the piezoelectric charge.

The two transducers were tested as cantilever beams at horizontal position, subjected to the following tests:

– PVDF transducer subjected to base vibration, and combined base excitation and flow induced vibration at characteristic points of high oscillation amplitudes.

Table 3: Comparative mechanical and thermal properties of the different material layers employed in the design of the PVDF (first 4 columns) and the PZT (last 3 columns) transducer.

Properties	Units	Mylar	Silver paint	PVDF	Acrylic	FR4	Copper	PZT
Young's modulus	GPa	5	70	3	2.5	26	110	79
Poisson's ratio		0.25	0.38	0.34	0.35	0.17	0.34	0.31
Density	kg/dm^3	1.39	10.5	1.77	1.41	1.9	8.93	7.9
Ultimate tensile strength	MPa	200	150	53.5	65	368	210	231
Tensile yield strength	MPa	107	35	10	35	340	33.3	90
Thermal expansion coefficient	μm/m-C	17	20	120	100	15	16.4	34.3

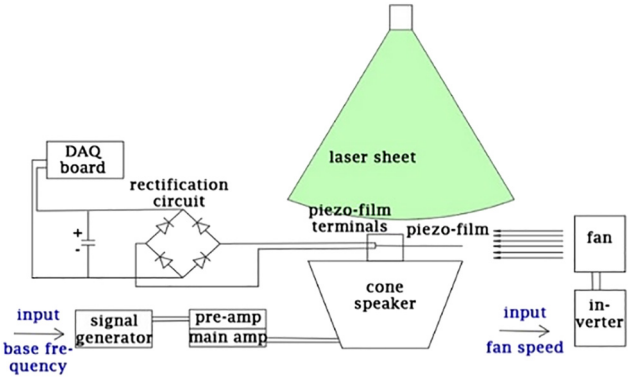

Figure 2: Schematic diagram of the experimental test rig set up for the combined excitation of the transducers.

- PVDF transducer with a 0.78 g tip mass, subjected to base vibration only in the vicinity of resonance
- PZT transducer with a 1.38 g tip mass, subjected to base vibration only

Beam curvature measurements

A line type laser was used to monitor the piezo-film's tip deflection and the cone speaker's vibration amplitude. The laser highlighted the moving beam's projection which was captured with long-exposure photography with a Nikon D3400 camera. Measurements of the film's tip deflection and the base's amplitude were made with an image processing tool in Matlab/Octave (Stamatellou 2021; Stamatellou and Kalfas 2021). The two extrema (upper and lower) of the transducer's and base's oscillation were captured by photographing the laser sheet projection with 1 s exposure (Stamatellou 2021). A projection of a high power output oscillation of the PVDF transducer is presented in Figure 4a. A respective projection of the PZT transducer's oscillation is seen in Figure 4b.

One of the main objectives of this work is to assess the conditions of maximum power harvesting capacity and maximum conversion efficiency of the transducers. According to the methodology presented in (Stamatellou 2021), the energy output per oscillation quadrant may be considered to be proportional to the total strain of the piezo-beam as it goes from neutral to full flexure position. As a consequence, to maximize the output of the piezo-transducer, it is necessary to maximize the product: (Frequency of oscillation) × (strain energy stored at the points of maximum tip deflection). Digitization of the curvature κ of the elastic curve's extrema extracted from image processing of the linear laser photographs is performed, since the curvature of the flexure curve is related to the bending moment M (Figure 5) by the equation:

$$\kappa = \frac{y''}{1 + (y')^2]^{\frac{3}{2}}} = \frac{M}{EI} \tag{1}$$

where κ is the beam's curvature at each point, E is the Young's modulus, I is the moment of inertia of the beam's cross section and $\boldsymbol{y}$ is

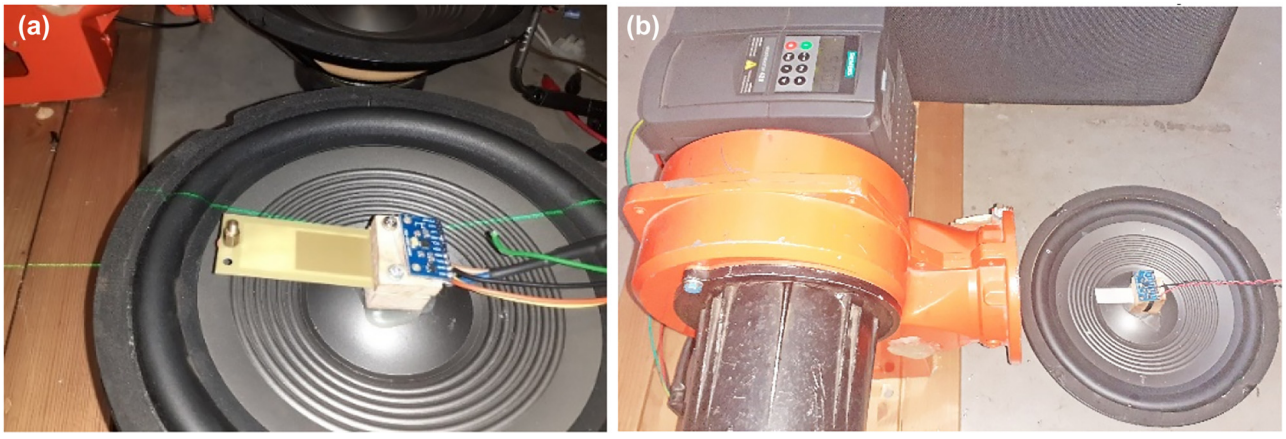

Figure 3: Placement of the PZT and PVDF transducers on the test rig. (a) PZT transducer at the test rig, with the tip mass for base only excitation, (b) PVDF transducer at the test rig, subjected to combined excitation.

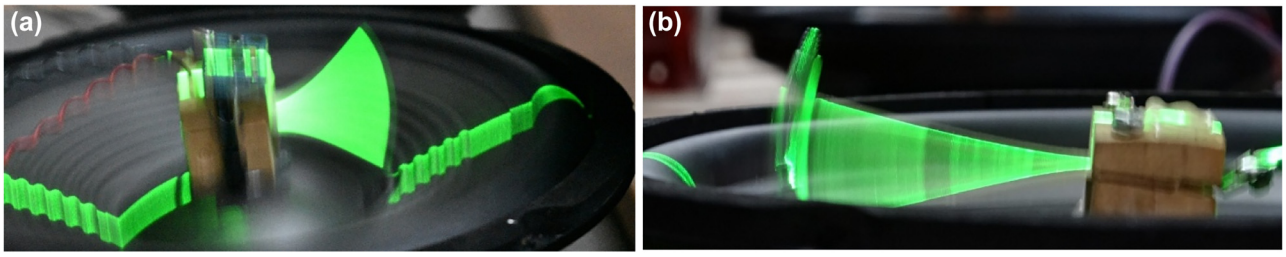

Figure 4: Laser sheet visualization of the LDT1 (PVDF) and S128 (PZT) transducer's oscillations with high harvested power. (a) LDT1 transducer, (b) S128 transducer.

the ordinate of the elastic curve. Then the elastic strain energy E_S of the piezo-beam at its two oscillation extrema is calculated by integration of its expression as function of the beam's curvature over its length, at specific time instances (t_{max}, t_{min}):

$$E_S(t_{max}) = \int_0^L \frac{1}{2} B\kappa(s, t_{max})^2 ds \quad (2)$$

$$E_S(t_{min}) = \int_0^L \frac{1}{2} B\kappa(s, t_{min})^2 ds \quad (3)$$

In these expressions, B is the flexural rigidity of the beam:

$$B = \frac{Eh^3}{12(1-\nu^2)} \quad (4)$$

where h is the beam's thickness, E the beam material's Young's modulus and ν its Poisson's ratio.

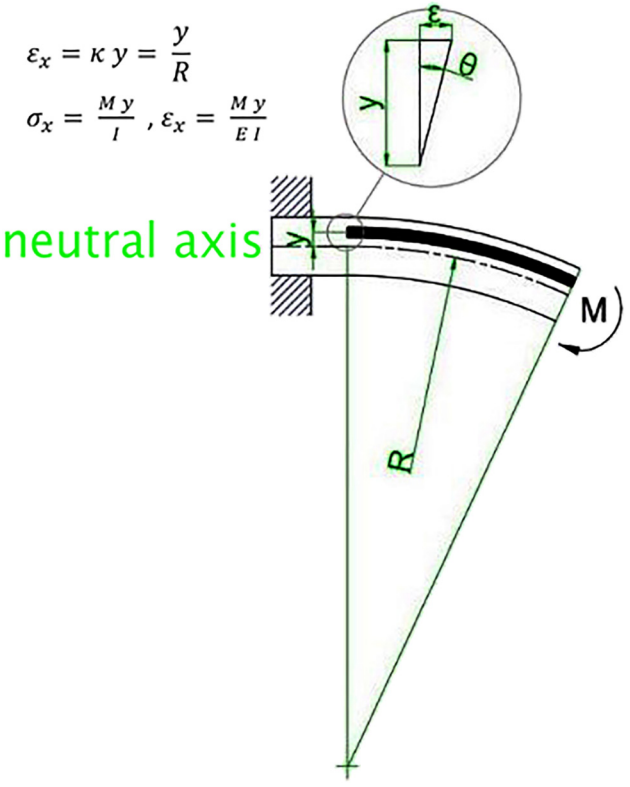

Figure 5: Correlation of beam curvature to stress and strain.

Thus, a conversion efficiency for a given charging time interval Δt_{ch} may be defined as the ratio of the electric-field energy accumulated by the supercapacitors, over the total elastic energy strain energy change of the material:

$$\eta = \frac{\frac{1}{2}CV^2}{2f\Delta t_{ch}[E_S(t_{max}) - E_S(t_{min})]} \quad (5)$$

where f denotes the vibration frequency and the expression in parentheses in the denominator is the difference in the beam's elastic strain energy values at the upper and lower vibration extrema.

Results and discussion

In the tests with the PVDF transducer, the supercapacitor's charging curves during 18,000 s have been recorded for the following three characteristic excitation modes and conditions:

(i) at 40 Hz base excitation only,
(ii) at 40 Hz base excitation combined with flow excitation with the fan at 1840 rpm speed and
(iii) at 12 Hz base excitation only, with a modified transducer (added 0.78 g magnetic tip mass).

All three excitation modes are known to produce high amplitude oscillations, being close to the modified transducer's natural frequencies (Stamatellou 2021). The forced vibrations result in the transducer oscillations frequency equal to the base excitation frequency, as confirmed by high speed photography (Stamatellou 2021). The evolution of the average capacitor charging rates was computed based on these curves and presented in Figure 6. As stated in the specialized literature and the manufacturer's data (Brown 2013), initial charging cycles from zero voltage have a low charging rate in the simple diode-bridge circuit (low efficiency). Subsequently, as shown in the Figure, the capacitor charging rate is continuously increasing, to stabilize after 14,000 s for all excitation frequencies. The stabilized average capacitor charging rate reaches 39 μW for the 40 Hz base excitation only and 43 μW for the combined 40 Hz base and 1840 rpm fan aerodynamic

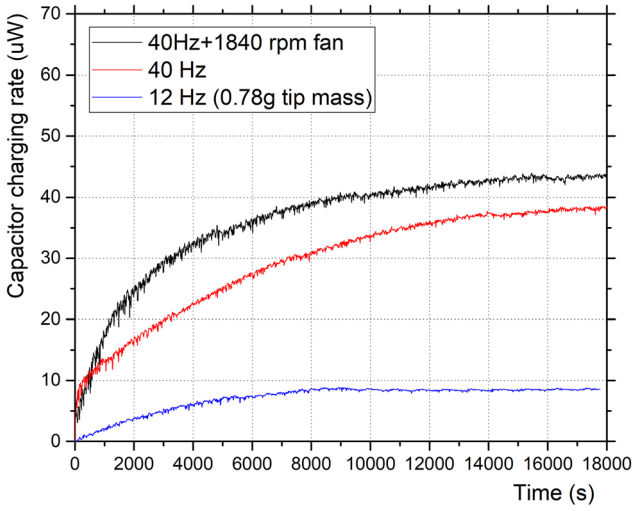

Figure 6: Charging rate of the 16 V/1.66 F capacitor from LDT1-028K transducer at characteristic excitation modes.

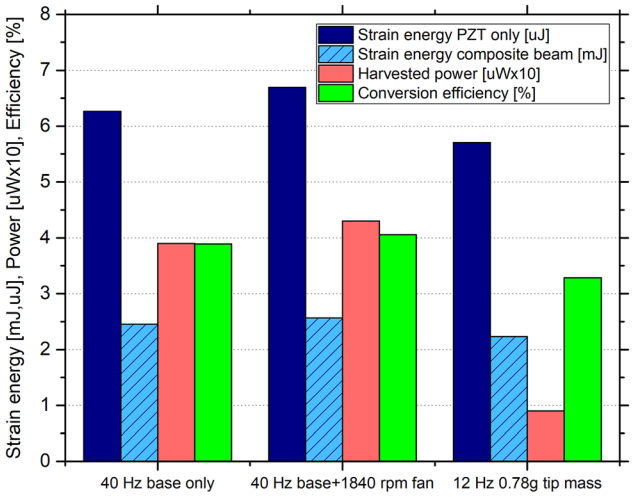

Figure 7: Comparison of the LDT1-028K transducer's harvested power and efficiency at three excitation modes: 40 Hz base excitation, combined excitation (40 Hz base + 1840 rpm fan) and transducer with 0.78 g tip mass at 12 Hz base excitation only.

excitation. The maximum output power of 43 μW, should be normalized to the volume of the piezoelectric material, in order to be comparable with the results of actuators of different sizes. According to the dimensions of Figure 1, the volume of PVDF piezoelectric material in the LDT1 transducer is $(12.2 \times 30 \times 0.028) = 10.25\ mm^3$. Dividing the output power by this volume corresponds to $4.2\ \mu W/mm^3$ which lies at the high end of the reported power output with PVDF piezoelectric transducers (Chang et al. 2010; Park et al. 2017). In comparison, the stabilized average capacitor charging rate reaches 9 μW for the 12 Hz base excitation only of the modified transducer with the 0.78 g tip mass.

The results of the strain energy and efficiency calculations for the specific operation points are summarized in Figure 7. For each operation point, the strain energy stored in the beam at its extremum point of oscillation is reported, along with the part of the strain energy stored inside the PVDF layer. Additionally, the efficiency calculated according to the above methodology and the harvested power at each operation point are presented. Comparison of the first two points with the 40 Hz base excitation indicates that the combined excitation mode significantly increases the harvested power and the strain energy at extremum points of oscillation. Efficiency is not significantly affected, lying around 4%. On the other hand, base excitation at 12 Hz of the modified transducer results in equally high strain energy stored at oscillation's extrema. The harvested power is significantly lower due to the lower frequency of oscillation. Efficiency remains at the same levels.

The respective tests with the S128 PZT transducer involved energy harvesting with base excitation only, in the frequency range of 50–61 Hz. Following the previously defined procedure, the evolution of the average supercapacitor charging rates was recorded and the stabilized values are plotted in Figure 8, as function of the base vibration frequency. According to the results with this transducer (Figure 8), the maximum stabilized average capacitor charging rate reaches 2.7 mW for a base excitation of 57 Hz. One additional test was performed at the specific base excitation frequency of 57 Hz, this time with increased amplifier gain. As seen in Figure 8, the output increased to 4.5 mW (red dot marker) when the maximum safe amplifier gain was selected. Further increasing amplifier gain would result to

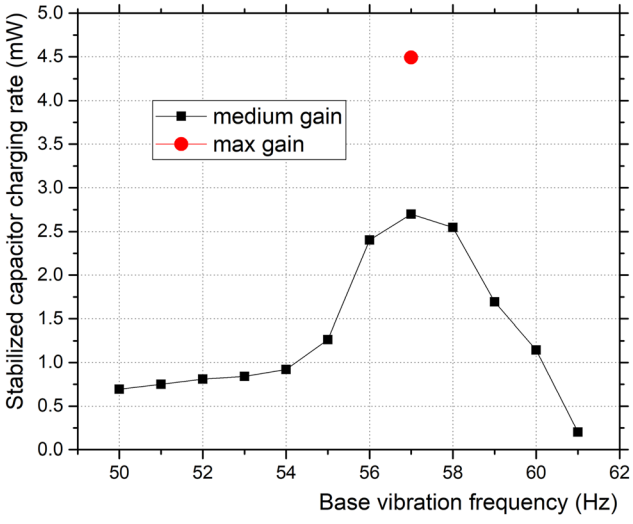

Figure 8: Charging rate of the 16 V/1.66 F super-capacitor, S128 PZT transducer (PZT) with 1.38 g tip mass for base excitation in the range 50–61 Hz.

high vibration amplitudes of the transducer's tip, causing it to collide to the speaker's membrane and fail.

Compared to the PVDF transducer, a nearly 100-fold increase in power output is observed. Next, the computation of strain energy at oscillation extrema was performed, in order to compute energy conversion efficiency for the PZT transducer and compare to the previously obtained values for the PVDF transducer. Again, the elastic strain energy was computed for these points based on the curvature of the flexure curves according to the above equations and the change of elastic strain energy between the two oscillation extrema (see Figure 4b).

The energy conversion efficiency for the maximum gain point at 57 Hz base vibration frequency is computed to 5% (Figure 9, left) and agrees with what is reported in (Stamatellou 2021) for a different excitation frequency range. Based on the technical data presented in Figure 1, the volume of PZT piezoelectric material that is incorporated in the S128 transducer is $(20.8 \times 46 \times 0.15)\ \text{mm}^3 = 143.5\ \text{mm}^3$. As already reported above, the respective volume of PVDF piezoelectric material in the LDT1 transducer is $10.25\ \text{mm}^3$. Thus the piezoelectric material of the PVDF transducer is 14 times less (per volume). A comparison of the best performance obtained with the two transducer types is summarized in Table 4. The PZT transducer attained a maximum of 4.5 mW at 57 Hz base excitation, while the PVDF transducer produced a maximum of 0.043 mW with combined excitation. Thus, maximum power per unit volume is 31 $\mu\text{W/mm}^3$, compared to 4.2 $\mu\text{W/mm}^3$ of the PVDF transducer.

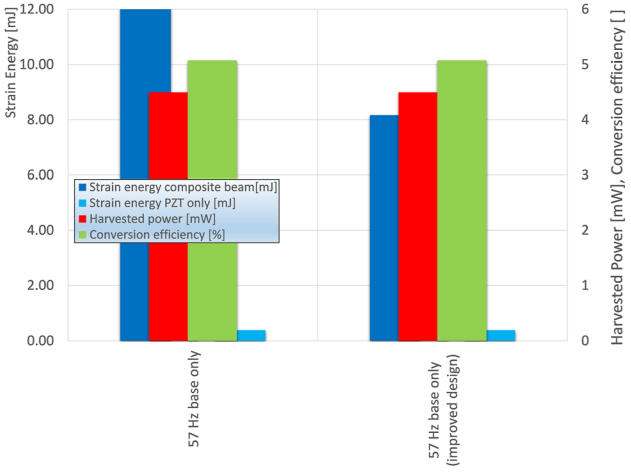

Figure 9: Harvested power and efficiency of the S128 transducer (1.38 g tip mass): stabilized capacitor charging rate with 57 Hz base excitation (left). Predicted behavior of modified transducer (right). Tip mass adapted to 1.0 g to match resonance frequency.

It is interesting to compare the efficiency values determined according to the above assessment methodology, with an approximate relation from the theory of piezoelectricity, which relates the conversion efficiency from mechanical to electrical energy by a piezoelectric patch placed on a horizontal cantilever beam and subjected to bending by the following relation (Brown 2013):

$$\eta = \frac{U_e}{U_m} = \frac{d_{31}^2}{\epsilon} E \tag{6}$$

For typical PVDF film, the above approximate formula gives an efficiency of about 2%, assuming a typical value of piezo coefficient $d_{31} = 25$ pC/N, a typical value for Young's Modulus $E = 3$ GPa and a typical value for DC dielectric permittivity $\varepsilon = 107 \times 10^{-12}$ F/m. On the other hand, the respective result for PZT with $E = 79$ GPa, $d_{31} = -270$ pC/N and $\varepsilon = 2.35 \times 10^{-8}$ F/m is close to 25% efficiency. Such differences between the performance of the piezoelectric material versus the full harvester, have been discussed by Lesieutre as early as 1997 (Lesieutre and Davis 1997). According to Chang et al. (Chang et al. 2010), the early onset of the nonlinear domain wall motions behavior has been identified as one mechanism responsible for the apparent high piezoelectricity measured in nanofibers of PVDF. Kim et al. (Kim et al. 2015) studied nanosheet-based piezoelectric nanogenerator with different thicknesses and types of dielectric layers and demonstrated that a careful design of the dielectric layer is necessary to improve the electrical outputs of piezoelectric nanogenerators (Chiu et al. 2018; Sachin, Haridass, and Ramanujam 2020). The efficiency levels for the PVDF transducer broadly agree with the above approximate calculation and with the data most frequently reported in the literature (Amini, Emdad, and Farid 2014; Bernard et al. 2017; Park et al. 2017; Uddin, Alford, and Aziz 2021), if one additionally takes into account that the experiments are usually

Table 4: Performance comparison between the two different transducer types tested.

Type	Resonance frequency (Hz)	Maximum harvesting frequency (Hz)	Maximum harvesting power (mW)	Maximum specific harvesting power (μW/mm3)
LDT1(PVDF)	58	40	0.043	4.2
S128 (PZT)	57 (1.38 g tip mass)	57 (1.38 g tip mass)	4.5	31

performed with small capacitors, or resistive circuits and definitions of efficiency vary among research groups (Stamatellou and Kalfas 2021). However, the efficiency values determined for the PZT transducer of the order of 5%, are significantly lower than the above figures predicted by Eq. (9). On the other hand, the well-known superiority of the PZT material to PVDF as regards energy harvesting potential per unit volume (Song et al. 2017; Yang, Erturk, and Zu 2017) is confirmed in these tests. Now, as regards the electrical energy output of the piezoelectric transducer, theory considers it to be proportional to the volume of the piezoelectric material incorporated in the transducer, and to the square of the applied strain (Brown 2013):

$$U_{\mathrm{e}} = \frac{1}{2}\eta V_{\mathrm{PVDF}} E \epsilon^2 \tag{7}$$

where η is the conversion efficiency from mechanical to electrical energy, E is the Young's modulus of the material, ε the strain and V_{PVDF} the volume of the piezoelectric material.

By normalizing to the area of the PVDF sheet incorporated in the transducer, we see that the normalized power output per unit area is proportional to the square of the applied strain and the thickness of the PVDF sheet (t_{PVDF}) employed in the construction of the transducer:

$$\frac{U_{\mathrm{e}}}{A} = \frac{1}{2}\eta t_{\mathrm{PVDF}} E \epsilon^2 \tag{8}$$

As regards the PZT transducer, indicative limits of harvested power are given by the manufacturer for a (10 × 10 × 0.25 mm) PZT-5A ceramic patch, subjected to a sinusoidally varying uniform strain ranging from 0 to 500 μstrain for a range of oscillation frequencies (Carter and Kensley 2020). The maximum strain in the tests performed in this study can be computed as the product of the curvature at maximum deflection and the distance of the PZT layer from the neutral line in bending. Since the minimum radius of curvature attained was 0.16 m and average y = 0.08 mm, average strain is 500 μstrain, that is, up to the upper limit given in the manufacturer's chart (Carter and Kensley 2020). The estimated harvested power for 57 Hz frequency of oscillation exceeds 5 mW for the specimen, or 0.2 mW/mm^3, which reduces to 0.03 mW/mm^3 after applying reductions according to the manufacturer's guidelines, because strains/stresses are not uniform in bending, never applied without loss, and electronic regulation circuits are not perfect. The measured result of 0.031 mW/mm^3 in bending is about the same level as the above figure prescribed by the manufacturer. As regards the PVDF transducer, the minimum radius of curvature was 0.0168 m and average y = 0.037 mm, resulting to 1500 μstrain. Thus, average strain at oscillations extrema is 3 times that of the PZT transducer. Maximum permissible strain limits with the PVDF material are 10,000–20,000 μstrain or 1–2%, which are not attainable with cantilever beam's configurations.

Proposed design modifications

The calculation of strain energy of the piezo-beam at its vibration extrema during the various forms of excitation, may be employed in a preliminary calculation of its energy harvesting potential. The superiority of the PZT over the PVDF material in piezoelectric energy harvesting capacity reported in the literature is confirmed in the specific comparative tests. On the other hand, by comparison of the elastic strain energy applied to each one of the two transducers, (examining the composite structure and not only the piezoelectric layer), it is observed from Figure 9 (left) that the elastic strain energy per half cycle that is required to excite the PZT transducer at its point of maximum power output, is about 30 times higher than the power absorbed by the PZT layer. This is a waste of power that is caused by the significant thickness (and stiffness) added to the PZT layer to protect the brittle ceramic, which failed twice during the tests with the PZT transducers. As regards the PVDF transducer, its protective Mylar layer is also relatively thick in order to protect the thin PVDF layer. It can be seen in the data reported in Figure 7 that the elastic strain energy per half cycle that is required to excite the PVDF transducer at its point of maximum power output, is about 300 times higher than the power absorbed by the PVDF layer. Thus, it would make sense to reduce the protective layer's thickness whenever a novel design of PVDF transducers emerge. Reduction of the laminate thickness to 3 mils instead of 5 mils for the Mylar layer, would make the elastic strain energy per half cycle only 190 times higher than the power absorbed by the PVDF layer. An acceptable durability for such a new design remains to be confirmed by extensive testing, with good prospects, since the current LDT1-028K transducer design version proved extremely durable in the experiments with no failures recorded in hundreds of hours of harsh testing (Stamatellou 2021). As regards the eigenfrequency, a pre-assessment of the performance of the modified design versions can be based on employing the approximate relation for the natural frequency of the slender beam:

$$\omega_{\mathrm{n}} = \sqrt{\frac{E}{\rho}} \tag{9}$$

where the composite beam's effective Young's Modulus and density are calculated as follows, for two layers of different materials 1, 2 with thickness of T_1 and T_2 respectively:

$$E = \frac{T_1E_1 + T_2E_2}{T_{\text{total}}}$$
$$\rho = \frac{T_1\rho_1 + T_2\rho_2}{T_{\text{total}}} \quad (10)$$

and the respective approximate relation for the slender beam of spring constant k with a tip mass m:

$$\omega_n = \sqrt{\frac{k_{sp}}{m}} \quad (11)$$

where the beam's spring constant k_{sp} can be calculated by the following relation:

$$k_{sp} = \frac{3EI}{L^3} \quad (12)$$

The proposed design of Figure 10a, reduces the thickness of FR4 layer in the downside of the S128 transducer from 0.36 to 0.028 mm and the thickness of the one to the upper side from 0.08 to 0.06 mm. This would result in the reduction of the total thickness of the transducer from 0.66 to 0.55 mm and its spring constant k from 0.306 to about 0.21 N/mm. In this way, its natural frequency would reduce to 85 Hz from 101 Hz, without the use of a tip mass. A tip mass of 1.00 g would further reduce the natural frequency to 57 Hz to match the design of the initially tested specimen. The new design would attain significantly higher overall energy conversion frequency, since the total strain energy stored in the composite beam is now only 20 times higher than the energy stored in the PZT layer (Figure 9 right). Another performance improvement could be attained by doubling the free oscillating length of this transducer, which would result to its dimensionless bending stiffness to a value lower than 1.0 (Figure 11) which would make it susceptible to flow induced excitation and thus further

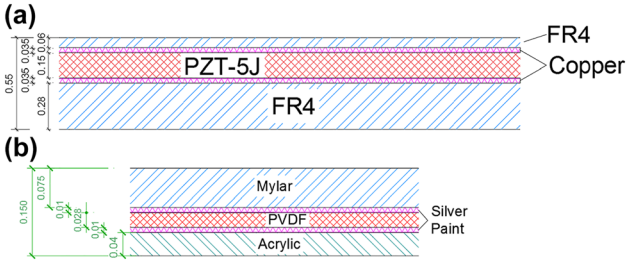

Figure 10: Proposed design modification (a) of the S128 transducer and (b) of the LDT1 transducer.

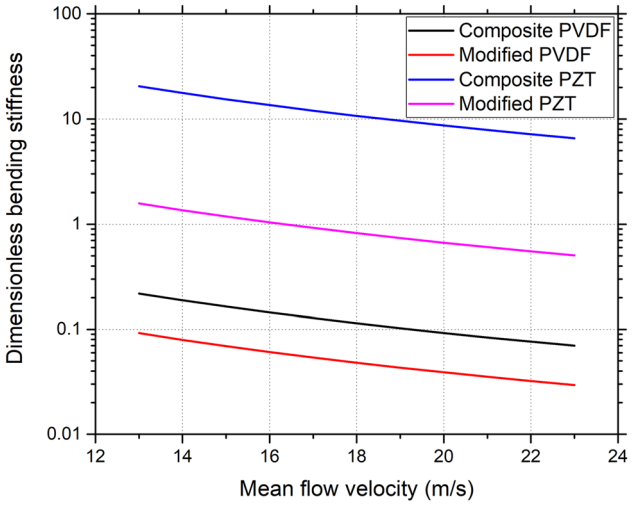

Figure 11: Dimensionless bending stiffness of initial and modified design of PVDF and PZT transducers tested in the existing flow excitation test rig (modified version of the PZT transducer is double in length).

improve its overall performance in combined excitation mode. The dimensionless bending stiffness is a critical parameter predicting the vibration of an inverted flag (Kim et al. 2013), comparing the bending force to the fluid inertial force:

$$\beta = \frac{E \cdot h^3}{12 \cdot \rho_f \cdot U^2 \cdot L^3 (1 - \nu^2)} \quad (13)$$

where E is the Young's modulus, ρ_f is the fluid density, ν is the film's Poisson's ratio, U is the mean flow velocity, h is the film's thickness and L its fluctuating length. If β is in the range $0.1 \le \beta \le 0.3$ then the film has a sustained flapping (Kim et al. 2013). As regards the PVDF transducer, its lamination procedure may also profit from the use of thinner Mylar layer. Here, instead of the 5 mil sheet, it is proposed to use the thinnest available Mylar sheet of 3 mil thickness (75 μm), which retains a sufficient bending stiffness (a 2 mil Mylar sheet not being capable to retain it). The modified transducer has its total thickness reduced from 200 to 150 μm, which would result to a reduction of its spring constant k from 0.005 to 0.002 N/mm. In this way, its natural frequency would reduce to 37 Hz from 57 Hz and its reduced bending stiffness will allow it to flutter with lower flow velocities (Figure 11), thus increasing the effect of combined excitation. Figure 11 presents the dimensionless bending stiffness range (computed according to Eq. (13)) for the specific test rig, for the standard and modified design versions of the PVDF and the PZT transducers. If the modified PZT transducer's length is doubled, it would be close to the range which enables flow induced excitation. Another benefit

from this thickness reduction would be a significant increase of the percentage of elastic strain energy of the composite structure eventually stored in the piezoelectric material and a respective increase in the effective energy conversion efficiency of the device.

Conclusions

Comparative tests were performed with a piezoelectric energy harvesting system based on two commercial piezoelectric transducers: The LDT1-028K, PVDF transducer, subjected to aerodynamic and base excitation in various combinations, produced a maximum harvested power output of 43 μW charging a super capacitor array, corresponding to a specific power of 4.2 $\mu W/mm^3$ which is at the high end of the reported output of PVDF piezoelectric transducers. The S128-J1FR-1808-YB, PZT transducer subjected to base excitation, produced an output of 4.5 mW which is comparable to that of the best-performing piezoceramic-based energy harvesters, and a power density of 31 $\mu W/mm^3$. The combinations of excitation that produced the highest beam curvature had the highest power outputs for both types of transducers. The curvature of the mode shapes was confirmed as an accurate predictor of the harvested power output. In this context, a novel definition of energy conversion efficiency is employed, based on the beam's curvature at its oscillation extrema, allowing for a fair assessment that is not dependent on the modelling accuracy of the beam's behavior. Moreover, the measured efficiency of a specific transducer can be employed in the prediction of its performance after specific design modifications of the composite structure. The significant efficiency superiority of the PZT transducer over the PVDF known from theory, was not observed in terms of the specific definition of efficiency. The test rigs and processing methods adopted, enable a fast screening and performance mapping of different types of PEHs, to focus on optimum energy harvesting efficiency and assessment of modified design versions to fit specific energy harvesting applications.

Acknowledgments: The author wants to thank ELPE – Hellenic Petroleum S.A. for financial assistance in this work.

Author contribution: All the authors have accepted responsibility for the entire content of this submitted manuscript and approved submission.

Research funding: None declared.

Conflict of interest statement: The authors declare no conflicts of interest regarding this article.

References

Aboulfotoh, N., and J. Twiefel. 2017. "A Study on Bandwidth and Performance Limitations of Array Vibration Harvester Configurations." *Energy Harvesting and Systems* 4 (1): 47–56.

Aboulfotoh, N., J. Twiefel, M. Krack, and J. Wallaschek. 2017. "Experimental Study on Performance Enhancement of a Piezoelectric Vibration Energy Harvester by Applying Self-Resonating Behavior." *Energy Harvesting and Systems* 4 (3): 131–6.

Amini, Y., H. Emdad, and M. Farid. 2014. "An Accurate Model for Numerical Prediction of Piezoelectric Energy Harvesting from Fluid Structure Interaction Problems." *Smart Materials and Structures* 23 (9): 095034.

Bernard, F., L. Gimeno, B. Viala, and O. Cugat. 2017. "The Effect of Temperature and Strain on Power Conversion Efficiency of PVDF-Based Thermal Energy Harvesters." *Proceedings* 1 (4): 1–4.

Bibo, A., and M. F. Daqaq. 2013. "Energy Harvesting under Combined Aerodynamic and Base Excitations." *Journal of Sound and Vibration* 332 (20): 5086–102.

Brenes, A., A. Morel, D. Gibus, C. S. Yoo, P. Gasnier, E. Lefeuvre, and A. Badel. 2020. "Large-Bandwidth Piezoelectric Energy Harvesting with Frequency-Tuning Synchronized Electric Charge Extraction." *Sensors and Actuators A: Physical* 302, https://doi.org/10.1016/j.sna.2019.111759.

Brown, R. H. 2013. *Piezo Film for Energy Harvesting*. London: Embedded Sensing Technologies.

Carter, R., and R. Kensley. 2020. *Introduction to Piezoelectric Transducers*. Woburn, MA, USA: piezo.com.

Chang, C., V. H. Tran, J. Wang, Y.-K. Fuh, and L. Lin. 2010. "Direct-Write Piezoelectric Polymeric Nanogenerator with High Energy Conversion Efficiency." *Nano Letters* 10 (2): 726–31.

Chiu, F.-C., Y.-C. Chuang, S.-J. Liao, and Y.-H. Chang. 2018. "Comparison of PVDF/PVAc/GNP and PVDF/PVAc/CNT Ternary Nanocomposites: Enhanced Thermal/Electrical Properties and Rigidity." *Polymer Testing* 65: 197–205.

Dai, H. L., A. Abdelkefi, and L. Wang. 2014. "Piezoelectric Energy Harvesting from Concurrent Vortex-Induced Vibrations and Base Excitations." *Nonlinear Dynamics* 77 (3): 967–81.

Elahi, H. 2021. "The Investigation on Structural Health Monitoring of Aerospace Structures via Piezoelectric Aeroelastic Energy Harvesting." *Microsystem Technologies* 27 (7): 2605–13.

Fan, Y., M. H. Ghayesh, and T.-F. Lu. 2020. "Enhanced Nonlinear Energy Harvesting Using Combined Primary and Parametric Resonances: Experiments with Theoretical Verifications." *Energy Conversion and Management* 221: 1–12.

Khazaee, M., A. Rezaniakolaie, A. Moosavian, and L. Rosendahl. 2019. "A Novel Method for Autonomous Remote Condition Monitoring of Rotating Machines Using Piezoelectric Energy Harvesting Approach." *Sensors and Actuators A: Physical* 295: 37–50.

Kim, D., J. Cossé, C. Huertas Cerdeira, and M. Gharib. 2013. "Flapping Dynamics of an Inverted Flag." *Journal of Fluid Mechanics* 736: R1–R12.

Kim, G. H., D.-M. Shin, H.-K. Kim, Y.-H. Hwang, and S. Lee. 2015. "Effect of the Dielectric Layer on the Electrical Output of a ZnO Nanosheet-Based Nanogenerator." *Journal of the Korean Physical Society* 67 (11): 1920–4.

Krishnamoorthy, K., P. Pazhamalai, V. K. Mariappan, S. S. Nardekar, S. Sahoo, and S.-J. Kim. 2020. "Probing the Energy Conversion Process in Piezoelectric-Driven Electrochemical Self-Charging

Supercapacitor Power Cell Using Piezoelectrochemical Spectroscopy." *Nature Communications* 11 (1): 2351.

Lesieutre, G. A., and C. L. Davis. 1997. "Can a Coupling Coefficient of a Piezoelectric Device Be Higher Than Those of Its Active Material?" *Journal of Intelligent Material Systems and Structures* 8 (10): 859–67.

Lu, Y., Y. Jiang, Z. Lou, R. Shi, D. Chen, and G. Shen. 2020. "Wearable Supercapacitor Self-Charged by P(VDF-TrFE) Piezoelectric Separator." *Progress in Natural Science: Materials International* 30 (2): 174–9.

Mayekol Mayck, H. D., A. M. R. Fath El-Bab, E. Murimi, and P. Moukala Mpele. 2021. "A Human Heartbeat Frequencies Based 2-DOF Piezoelectric Energy Harvester for Pacemaker Application." *Energy Harvesting and Systems* 8 (1): 1–11.

Measurement_Specialties. 2008. *LDT with Crimps Vibration Sensor/ Switch Data Sheet.* Hampton, VA, USA: MS.

Nix, E. L., and I. M. Ward. 1986. "The Measurement of the Shear Piezoelectric Coefficients of Polyvinylidene Fluoride." *Ferroelectrics* 67 (1): 137–41.

Orrego, S., K. Shoele, A. Ruas, K. Doran, B. Caggiano, R. Mittal, and S. H. Kang. 2017. "Harvesting Ambient Wind Energy with an Inverted Piezoelectric Flag." *Applied Energy* 194: 212–22.

Park, S., Y. Kim, H. Jung, J.-Y. Park, N. Lee, and Y. Seo. 2017. "Energy Harvesting Efficiency of Piezoelectric Polymer Film with Graphene and Metal Electrodes." *Scientific Reports* 7 (1): 17290.

Priya, S., H.-C. Song, Y. Zhou, R. Varghese, A. Chopra, S.-G. Kim, I. Kanno, L. Wu, D. S. Ha, J. Ryu, and R. G. Polcawich. 2017. "A Review on Piezoelectric Energy Harvesting: Materials, Methods, and Circuits." *Energy Harvesting and Systems* 4 (1): 3–39.

Ramadoss, A., B. Saravanakumar, S. W. Lee, Y.-S. Kim, S. J. Kim, and Z. L. Wang. 2015. "Piezoelectric-Driven Self-Charging Supercapacitor Power Cell." *ACS Nano* 9 (4): 4337–45.

Sachin, M., R. Haridass, and B. T. S. Ramanujam. 2020. "Polyvinylidene Fluoride (PVDF)-poly(methyl Methacrylate) (PMMA)-Expanded Graphite (ExGr) Conducting Polymer Blends: Analysis of Electrical and Thermal Behavior." *Materials Today Proceedings* 28: 103–7.

Shu, Y. C., and I. C. Lien. 2006. "Efficiency of Energy Conversion for a Piezoelectric Power Harvesting System." *Journal of Micromechanics and Microengineering* 16 (11): 2429–38.

Song, J., G. Zhao, B. Li, and J. Wang. 2017. "Design Optimization of PVDF-Based Piezoelectric Energy Harvesters." *Heliyon* 3 (9): e00377.

Stamatellou, A.-M. 2021. "Investigation of Power Output and Efficiency of Piezoelectric Energy Harvesters." PhD Thesis, Aristotle University Thessaloniki. https://www.didaktorika.gr/eadd/handle/10442/50443.

Stamatellou, A.-M., and A. I. Kalfas. 2018. "Experimental Investigation of Energy Harvesting from Swirling Flows Using a Piezoelectric Film Transducer." *Energy Conversion and Management* 171: 1405–15.

Stamatellou, A.-M., and A. I. Kalfas. 2019. "Testing of Piezoelectric Energy Harvesters Isolated from Base Vibrations." *Energy Conversion and Management* 196: 717–28.

Stamatellou, A.-M., and A. I. Kalfas. 2020. "Piezoelectric Energy Harvesting Experiments under Combined Aerodynamic and Base Excitation." *Journal of Intelligent Material Systems and Structures* 32 (2): 169–81.

Stamatellou, A.-M., and A. I. Kalfas. 2021. "On the Efficiency of a Piezoelectric Energy Harvester under Combined Aeroelastic and Base Excitation." *Micromachines* 12 (8): 1–22.

Sun, W., F. Guo, and J. Seok. 2019. "Development of a Novel Vibro-Wind Galloping Energy Harvester with High Power Density Incorporated with a Nested Bluff-Body Structure." *Energy Conversion and Management* 197: 111880.

Sun, W., and J. Seok. 2020. "A Novel Self-Tuning Wind Energy Harvester with a Slidable Bluff Body Using Vortex-Induced Vibration." *Energy Conversion and Management* 205: 1–15.

Tam Nguyen, H.-D., H.-T. Pham, and D.-A. Wang. 2013. "A Miniature Pneumatic Energy Generator Using Kármán Vortex Street." *Journal of Wind Engineering and Industrial Aerodynamics* 116: 40–8.

Uddin, M., S. Alford, and S. M. Aziz. 2021. "Evaluating Energy Generation Capacity of PVDF Sensors: Effects of Sensor Geometry and Loading." *Materials* 14 (8): 1–17.

Vatansever, D., R. L. Hadimani, T. Shah, and E. Siores. 2011. "An Investigation of Energy Harvesting from Renewable Sources with PVDF and PZT." *Smart Materials and Structures* 20 (5): 055019.

Wang, L., L. Zhao, G. Luo, Y. Zhao, P. Yang, Z. Jiang, and R. Maeda. 2020. "System Level Design of Wireless Sensor Node Powered by Piezoelectric Vibration Energy Harvesting." *Sensors and Actuators A: Physical* 310: 1–10.

Yang, Z., A. Erturk, and J. Zu. 2017. "On the Efficiency of Piezoelectric Energy Harvesters." *Extreme Mechanics Letters* 15: 26–37.